Origin of Immediate Damping of Coherent Oscillations in Photoinduced Charge-Density-Wave Transition

Wen-Hao Liu,[1,2,*] Yu-Xiang Gu,[1,2,*] Zhi Wang,[1] Shu-Shen Li,[1,2] Lin-Wang Wang,[1,†] and Jun-Wei Luo[1,2,‡]
[1]State Key Laboratory of Superlattices and Microstructures, Institute of Semiconductors, Chinese Academy of Sciences, Beijing 100083, China
[2]Center of Materials Science and Optoelectronics Engineering, University of Chinese Academy of Sciences, Beijing 100049, China

(Received 8 September 2022; revised 16 February 2023; accepted 13 March 2023; published 7 April 2023)

In stark contrast to the conventional charge density wave (CDW) materials, the one-dimensional CDW on the In/Si(111) surface exhibits immediate damping of the CDW oscillation during the photoinduced phase transition. Here, we successfully reproduce the experimental observation of the photoinduced CDW transition on the In/Si(111) surface by performing real-time time-dependent density functional theory (rt-TDDFT) simulations. We show that photoexcitation promotes valence electrons from the Si substrate to the empty surface bands composed primarily of the covalent p-p bonding states of the long In-In bonds. Such photoexcitation generates interatomic forces to shorten the long In-In bonds and thus drives the structural transition. After the structural transition, these surface bands undergo a switch among different In-In bonds, causing a rotation of the interatomic forces by about $\pi/6$ and thus quickly damping the oscillations in feature CDW modes. These findings provide a deeper understanding of photoinduced phase transitions.

DOI: 10.1103/PhysRevLett.130.146901

Quasi-one-dimensional indium atomic wires grown self-assembly on a silicon (111) surface, denoted as In/Si(111), have recently been extensively studied both experimentally and theoretically [1–14] since Yeom *et al.* [1] reported a reversible metal-to-insulator transition (MIT). At room temperature, the self-assembled In atomic wires on a Si (111) surface are composed of a pair of parallel zigzag In chains separated by a zigzag Si chain [2], resulting in a (4×1) unit cell, as shown in Fig. 1(b). This phase is in a metallic state as featured by three strongly dispersive, partially occupied, quasi-1D surface bands [denoted by S_1, S_2, and S_3 in Fig. 1(d) and Supplemental Material Fig. S4(a) [15]]. Below $T_c = 125$ K, In atoms rearrange into distorted hexagons with an (8×2) reconstructed quadrupled unit cell [Fig. 1(a)] [3], accompanying the formation of a 1D charge density wave (CDW) [1] owing to strong coupling between electron density modulation and periodic lattice distortion. In contrast to the metallic (4×1) phase, the symmetry reduced (8×2) phase opens a band gap of 0.1–0.3 eV [1,4–7] at the $X_{8\times2}$ point and thus becomes an insulator [(Fig. 1(c)]. After a long pursuit, the structural transformation between the zigzag and hexagon patterns is recognized experimentally as a superposition of soft rotary and shear phonon modes [8–14]. These two phonon modes are also known as the CDW amplitude modes of the periodic lattice distortions [14]. Photoexcitation using ultrafast laser pulses has been recently demonstrated as an efficient route to manipulate MIT and to melt the 1D CDW in In/Si(111) on the timescale of lattice vibrations [13,14,18,27–32]. However, it exhibits rapid damping of the CDW mode oscillations during the photoinduced transition [18,32] in striking contrast to all the other CDW materials [33–36]. Despite the postulated possibilities of an energy barrier hindering the immediate sliding back into the CDW mode [32] or a strong damping of the CDW amplitudes through fast mode conversion caused by a rapid transfer of their energy to surface phonon modes of the Si substrate [18], the underlying microscopic mechanism remains ambiguous.

In this Letter, we aim to reveal the microscopic mechanism underlying the swift suppression of the coherent CDW amplitude-mode oscillations by performing advanced real-time time-dependent density functional theory (rt-TDDFT) simulations [16,17]. Our rt-TDDFT calculations, for the first time, reproduce the experimentally observed dynamics of photoinduced CDW transition in In/Si(111) without *ad hoc* assumptions. We illustrate that the photoelectron population of the empty S_1 and S_2 bands generates atomic forces that drive the motion of In atoms in CDW amplitude modes, resulting in the structural transition from the (8×2) phase to the (4×1) phase. We elucidate that the S_1 and S_2 bands are mainly from the bonding states of In bonds crossing two zigzag In chains in the (8×2) phase. However, in the (4×1) phase, the S_1 and S_2 bands switch to that within single zigzag In chains. Such bond switching prevents In atoms from motions in the CDW phonon modes via turning the direction of the atomic driving forces by about $\pi/6$.

Figure 1 shows the rt-TDDFT simulation of structural dynamics of photoinduced phase transition in the In/Si(111)

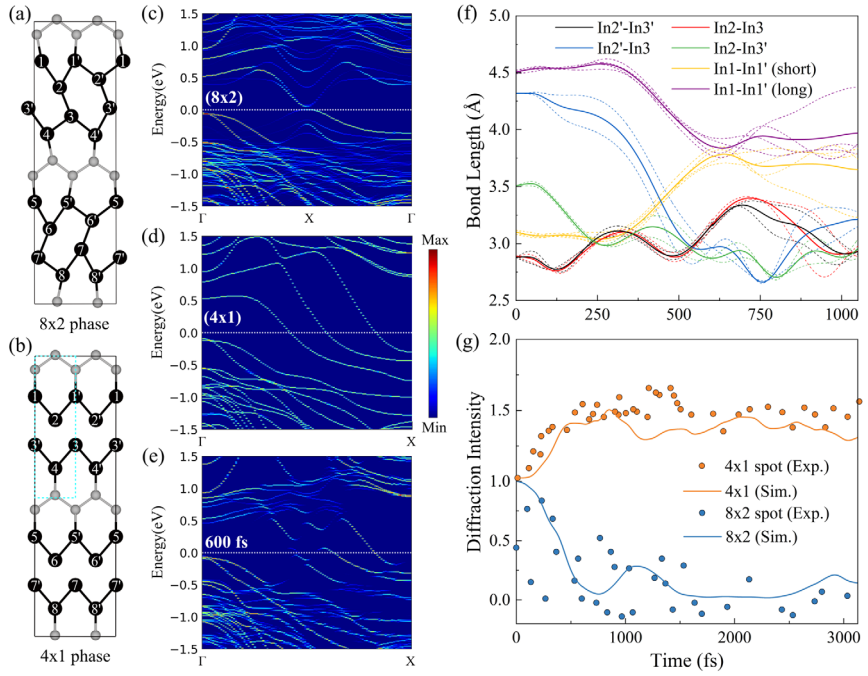

FIG. 1. The atomic configures of the In/Si(111) wire in (a) the hexagon (8 × 2) phase and (b) the zigzag (4 × 1) phase. The red dashed box in (b) indicates the (4 × 1) primary cell. The In atoms are numbered according to In lines from left to right, and the prime superscript is used to distinguish two neighbors In atoms in each line. In the (4 × 1) phase, each zigzag In chain is composed of two lines of In atoms. Calculated unfolded band structures of the (8 × 2) phase in (c), (4 × 1) phase in (d), and dynamic phase at 600 fs (e). (f) Dynamic evolution of the characteristic In-In bonds in the hexagon (8 × 2) phase following photoexcitation. (g) The time trajectory of the diffraction intensities of an (8 × 2) spot [indicative of the (8 × 2) structure] and a (4 × 1) spot [indicative of the (4 × 1) structure] obtained from our rt-TDDFT simulation in comparison with experimental data measured by ultrafast electron diffraction [37].

(8 × 2) surface under irradiation of 120 fs duration, 1.55 eV laser pulses with a fluence promoting about 3.4% of valence electrons from the valence bands to the conduction bands crossing the Fermi level E_f (Supplemental Material, note 1 and Fig. S1 [15]). We can see that it reproduces well the experimental observations [37]. The high-temperature zigzag (4 × 1) phase [Fig. 1(b)] has been recognized as connected to the low-temperature hexagon (8 × 2) phase [Fig. 1(a)] via the dimerizations of the outer In atoms in each zigzag In chain and of the inner In atoms across two zigzag In chains following the superposition of a shear distortion and two hexagon rotary distortions [9–14,38]. Figure 1(a) shows that the shear distortion between two zigzag In chains induces the dimerization of the inner In atoms as getting In 2-In 3, In 2'-In 3', In 6-In 7', and In 6'-In 7 bonds shorter (to 2.8 Å) and getting In 2-In 3', In 2'-In 3, In 6-In 7, and In 6'-In 7' bonds longer. The following hexagon rotary distortion further breaks the identical bond length of In 2-In 3'/In 2'-In 3 and In 6'-In 7'/In 6-In 7 pairs into longer (4.3 Å) and shorter bonds (3.5 Å), and simultaneously causes the dimerization of the outer In atoms by shortening the In 1-In 1' and In 5-In 5' bonds from 3.7 to 3.1 Å and elongating the In 4-In 4' and In 8-In 8' bonds from 3.7 to 4.5 Å. The atomic snapshots (shown in the Supplemental Material movie [15]) exhibit that two (4 × 2) hexagon building blocks in the (8 × 2) phase undergo transitions simultaneously from hexagon structure to zigzag structure. For the sake of simplicity, we will examine one of two (4 × 2) hexagon blocks hereafter (unless stated otherwise).

Figure 1(f) shows that, after the photoexcitation, the outer In dimers start dissolution at $t = 300$ fs, evidenced by the elongating of their bond lengths from $d_{1\text{-}1'} = d_{4\text{-}4'} = 3.1$ Å along with the shortening of their long counterparts from 4.5 Å. At $t = 600$ fs, the outer In dimers and their long counterparts have the same bond length as their equilibrium bond length (3.7 Å) in the zigzag (4 × 1) phase. In contrast, the dissociation of the inner dimers (In 2-In 3 and In 2'-In 3') begins (earlier) at 125 fs after undergoing a slight shortening following the photoexcitation. Meanwhile, their long counterparts (In 2'-In 3 and In 2-In 3' bonds) come into being shorter at 100 fs. Although the In 2'-In 3 bond ($d_{2'\text{-}3} = 4.3$ Å) is much longer than the In 2-In 3' bond ($d_{2\text{-}3'} = 3.5$ Å), they encounter a crossing in bond length at around 540 fs, approaching the same length as their equilibrium bond length ($d_{2'\text{-}3} = d_{2\text{-}3'} = 2.94$ Å) in the zigzag (4 × 1) structure. After getting crossed, a slight overshoot takes place as the continuously elongating of the inner dimers and shortening of their long counterparts until 750 fs. They then rebound slightly (but never fully back) toward the (8 × 2) structure. We deduce that the $(8\times2)-(4\times1)$ transition completes at around $t = 600$ fs, although the inner and outer In dimers reach their exact

equilibrium positions in the zigzag (4×1) phase at slightly different times ($t = 540$ and 600 fs, respectively). This deduction can be further confirmed by inspecting the snapshots of atomic configurations at $t = 60$, 220, 300, 400, 500, and 600 fs, as shown in Fig. 3(a) (a higher temporal resolution is also given in the Supplemental Material movie [15] accompanied by corresponding band structure). One can see that the atomic configuration at $t = 600$ fs is truly close to the zigzag (4×1) structure shown in Fig. 1(b), with deviation invisible to the naked eye. The band structure of the transient phase at 600 fs [Fig. 1(e)] exhibits three bands crossing the Fermi energy, a character feature of the (4×1) metal phase [Fig. 1(d)]. It also indicates the achievement of the photoinduced phase transition from (8×2) to (4×1) phase.

To make a direct comparison with the experimental electron diffraction, we calculate the time-dependent diffraction intensity based on the atomic trajectories produced by the rt-TDDFT simulations according to the Debye-Waller factor [19,20],

$$I(t) = \exp[-Q^2\langle u^2(t)\rangle/3], \tag{1}$$

where Q is the magnitude of the reciprocal lattice vector for the diffraction spot, and $u^2(t)$ is the squared displacement of atoms from their ideal lattice positions at time t (Supplemental Material Fig. S3 [15]). Figure 1(g) exhibits that the simulated diffraction intensities at both the (8×2) and (4×1) spots are in great agreement with the experimental data over the whole investigated period from 0 to 3000 fs. Specifically, the simulated diffraction intensity at the (8×2) spot drops sharply within 600 and at 750 fs reaches the minimum, which indicates the complete quenching of the hexagon (8×2) structure. Meanwhile, the diffraction intensity at the (4×1) spot grows quickly within 500 fs and then gradually increases to the maximum at 1000 fs. The slow increase of the (4×1) spot indicates the arrangement of the system in the vicinity of the zigzag (4×1) structure. Hence, we have demonstrated that the (8×2)-(4×1) structural transition deduced from the diffraction pattern is consistent with that obtained from the bond dynamics shown in Fig. 1(f).

Our rt-TDDFT simulation predicted that the photoinduced structural transition is completed around 600 fs, in excellent agreement with experimentally measured timescales of ~700 fs [18] and 660 ± 120 fs [13] from the lattice dynamics using time-resolved reflection high-energy electron diffraction (tr-RHEED) and of ~660 [13] and ~700 fs [29] from the band structure dynamics using time- and angle-resolved photoemission spectroscopy (tr-ARPES). From the band structure evolution shown in the Supplemental Material movie [15], we further find that the bandgap closure of the insulating (8×2) phase occurred at about 200 fs earlier than the completion of the structural transition, which is also consistent with the tr-ARPES observations [13,29]. Besides, Fig. 2 shows that the phase transition time rapidly decreases to a saturation value (~660 fs) with increasing electronic excitations in excellent agreement with the previous experiments [18]. It is commonly believed that the transition time is limited by a quarter of the atomic vibration period in combined frequencies: 0.54 THz (1852 fs) for shear mode and 0.81 THz (1235 fs) for rotary mode [18]. We obtain the two phonon modes at the ground state by using the dynamic matrix method. We further show the phonon softening in the excited state by two phonon modes projected to excited state phonon modes (Fig. S7). By projecting atom motions to these two phonon modes, Supplemental Material, Fig. S7 [15] shows these two phonon modes diminishing ultimately around 700 fs in our rt-TDDFT simulations, confirming the CDW amplitude modes connecting the (8×2) and (4×1) phases. Overall, we have theoretically reproduced the experimental observations of the photoinduced phase transition of In/Si(111) wires from the insulating (8×2) phase to the metallic (4×1) phase without *ad hoc* assumptions.

Notably, our rt-TDDFT simulations validate all experimental findings [13,18,30,32] that the diffraction intensity stabilizes without any indications of coherent oscillatory behavior after melting the 1D CDW phase in sharp contrast to the conventional photoinduced CDW transitions [18,36,39–43]. According to the Peierls picture, the photoinduced phase transitions are due to the photoexcitation of the displacive soft phonon modes that are connected to the lattice Peierls distortion. Because the damping of a phonon will take place on a much longer timescale than the phonon's period, these soft phonons will drive back-and-forth transitions between two transitional phases, generating coherent oscillation. In quasi-one-dimensional CDW $K_{0.3}MoO_3$ [39,40] and $Pr_{0.5}Ca_{0.5}MnO_3$ [41] as well as two-dimensional CDW 1T-$TiSe_2$ [36], 1T-TaS_2 [42], and 1T-$TaSe_2$ [43], the coherent oscillations in diffracted x-ray intensity controlled by photoexcitation

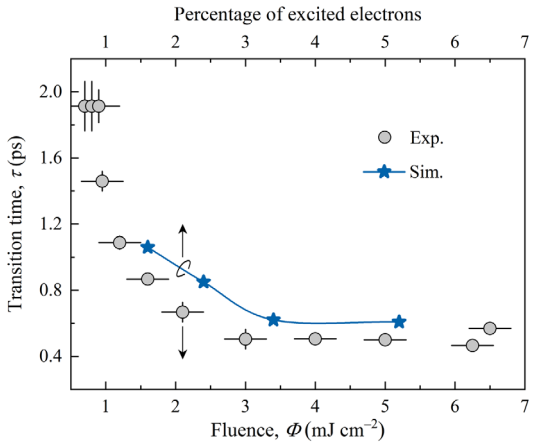

FIG. 2. The rt-TDDFT simulations predicted phase transition time τ from (8×2)-to-(4×1) phase as a function of the percentage of photoexcited electrons in comparison with experimental data as a function of the laser fluences [18].

have already been seen and discussed. In the In/Si(111) surface, the shear distortion (0.54–0.66 THz) and hexagon rotary distortion (0.81–0.84 THz) [9,11,12,14] are recognized as two displacive soft phonon modes (or CDW amplitude modes) that connect the hexagon (8×2) and zigzag (4×1) phases [13,14]. Therefore, the quick damping of the coherent oscillations is unexpected in the CDW phase transitions [36,39–43].

To understand the immediate damping of the coherent oscillations, we turn to inspect the photoinduced atomic forces driving atoms in collective and directed motions that give rise to the CDW amplitude phonon modes. Figure 3(b) shows the real-space distribution of photoexcited electrons (holes given in Supplemental Material, Fig. S5 and Fig. S6 [15]) that exhibits that the 1.55 eV femtosecond laser pulses promote electrons from the valence bands of Si substrate to the empty surface bands of the In/Si(111) (8×2) structure. Considering only a tiny portion of photoholes located in the regime of In wires, we expect photoelectrons rather than photoholes to be the primary factor driving the phase transition. This expectation contradicts the earlier AIMD simulations [18,29], which assume both photoexcited electrons and holes in equilibrium distribution with a much higher electronic temperature than the lattice temperature. Figure 3(b) shows that at 60 fs (just after the photoexcitation), the maximum occupancy of photoelectrons is on the In 2-In 3' bond with a tiny component on the In 2'-In 3 bond. Figure 3(a) shows that from 60 to 300 fs, only In 2 and In 3' among all In atoms undergo visible displacements. It implies that photoelectrons and structural evolution are highly correlated. We have elucidated that the S_2 and S_1 bands in the (8×2) phase mainly consist of the In $5p$ bonding states of the In 2-In 3' bond and the In 2'-In 3 bond, respectively (Fig. 4 and detailed in Supplemental Material, Fig. S4 [15]). A significant portion of photoexcited electrons initially occupies the high-lying S_2 band, generating attractive forces in the In 2-In 3' and In 2'-In 3 bonds because the excited system will gain energy from lowering the energy of occupied bonding states via shortening the bond length [19,21,44]. The generated interatomic force of the In 2-In 3' bond is stronger than that of the In 2'-In 3 bond due to its higher photoelectron density [19,20,45]. Subsequently, Fig. 3(a) shows that the attractive force pulls In 2 and In 3' atoms closer in a much larger magnitude than that between In 2' and In 3 atoms within 300 fs.

As the S_2 band goes down in energy accompanying the In 2-In 3' bond shortening, the hot photoelectrons in the high-lying S_2 band will relax to the low-lying S_1 band. It is indicated by the change of the maximum photoelectron occupation from the In 2'-In 3 bond to the In 2'-In 3 bond at 300 fs, as shown in Fig. 3(c). Such charge transfer remarkably enhances the attractive force in the In 2'-In 3 bond, which pulls the In 2' and In 3 atoms to move relative to one another along the bond [Fig. 3(a)] and thus shortening the In 2'-In 3 bond in the period from 300 to 500 fs [Fig. 1(c)]. Whereas, in this period, In 2 and In 3' atoms have no further movements due to the compensation of the photoinduced force by the enhanced electrostatic repulsion of electron clouds. At 600 fs, the system achieves the zigzag (4×1) phase [Fig. 3(d)] following the de-dimerization of the outer In dimers along with the direction of the boundary In-Si bonds switching perpendicularly to the In wire (detailed in the Supplemental Material movie [15]). Note

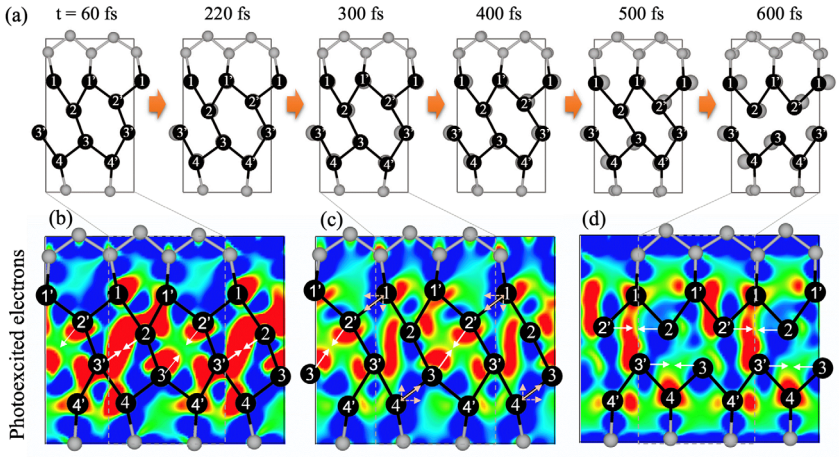

FIG. 3. Time evolution of atomic structure and photoexcited electrons of In/Si(111) in the (8×2) phase following photoexcitation. (a) Snapshots of atomic positions at 60, 220, 300, 400, 500, and 600 fs after photoexcitation. Big black dots represent In atoms (whose initial positions before photoexcitation are marked by grey color to guide the eye) and small gray dots for Si atoms. (b)–(d) The distributions of the photoexcited electrons at $t = 60$, 300, and 600 fs, respectively, following photoexcitation. The white arrows denote the photoexcitation-generated interatomic forces via the photoelectron population of surface conduction bands. Pink solid arrows in (c) indicate the forces pulling the In1 and In4 atoms resulting indirectly from the shrinkage of the In 2'-In 3 bond. Their decomposition components (vertical and horizontal directions) are represented by pink dashed arrows.

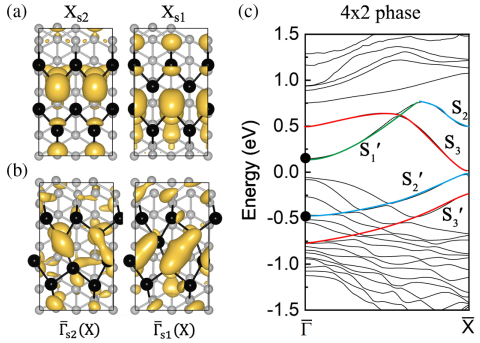

FIG. 4. The wave functions of the S_1 and S_2 bands at $X_{4\times1}$ point in the (4×1) phase (b) and in the (4×2) phase (c) in which they are folded to the $\bar{\Gamma}$ point, accompanying the top view of the corresponding atomic structure. Here, the black circles represent In atoms and the gray circles represent Si atoms. (c) First-principles band structure of the In/Si(111) (4×2) structure (half of the (8×2) structure).

that, during the (8×2) to (4×1) structural transition, In 1 (In 4) exhibits a leftward (rightward) displacement leaving behind its dimer's counterpart In 1' (In 4') having almost invisible displacement from its initial position. It implies that the atomic forces driving the movements of In 1 and In 4 arise indirectly from the shrinkage of the In 2'-In 3 bond, as indicated in Fig. 3(c). Their vertical components of atomic driving forces are compensated by Si—In bonds, leading to no vertical displacement.

Interestingly, Fig. 4 shows a switch of the S_1 and S_2 bands from the In $5p$ bonding states of In 2-In 3' and In 2'-In 3 dimers in the (8×2) phase to that of In 2-In 2' and In 3-In 3' bonds in the (4×1) phase, respectively (see Supplemental Material, note 4 for details [15]). It explains the rotation of the photoelectron distribution pattern as the system achieves the (4×1) phase at $t = 600$ fs, as shown in Figs. 3(b)–3(d). Subsequently, the directions of photo-induced atomic forces switch correspondingly to parallel to the In wire by a rotation of about $\pi/6$, as shown in Fig. 3(d). Thus, we have illustrated that a bond switch in surface bands is responsible for the disappearance of atomic forces driving the rebound back to the (8×2) phase, resulting in no oscillations of the CDW transition modes [13,18,32]. This microscopic viewe is somewhat related to the argument of an energy barrier hindering the immediate sliding back into the CDW mode [32] (Supplemental Materia, Fig. S7 [15]) but different from the argument of fast mode conversion caused by a rapid transfer of their energy to surface phonon modes of the Si substrate [18]. To explicitly assess the energy barrier, we calculate the dynamic potential energy surface (PES) following Refs. [25,26] obtained from the evolution of the kinetic energy in a nonadiabatic dynamic. The dynamic PES obtained from rt-TDDFT simulation for 3.4% photoexcitation (Supplemental Material, Fig. S10 [15]) exhibits multiple local minima, responding to electron-phonon coupling and multiphonon scattering, to dissipate oscillation.

In summary, we have successfully reproduced the experimental observations of photoinduced phase transition in the In/Si(111) (8×2) structure by performing advanced rt-TDDFT simulations. We find that the photoelectron population of the empty surface S_1 and S_2 bands generates atomic driving forces for the motion of In atoms in CDW amplitude modes, resulting in the transition from the (8×2) phase to the (4×1) phase. A bond switch in the surface S_1 and S_2 bands causes rotation of the atomic driving forces by about $\pi/6$, leading to the immediate damping of the CDW amplitude phonon modes.

The work was supported by the National Natural Science Foundation of China (NSFC) under Grants No. 11925407, No. 61927901, and No. 12204470, the Key Research Program of Frontier Sciences, CAS under Grant No. ZDBS-LY-JSC019, CAS Project for Young Scientists in Basic Research under Grant No. YSBR-026, the Strategic Priority Research Program of the Chinese Academy of Sciences under Grant No. XDB43020000, and the Key Research Program, CAS under Grant No. ZDBS-SSW-WHC002.

*These authors contributed equally to this work.
†lwwang@semi.ac.cn
‡jwluo@semi.ac.cn

[1] H. W. Yeom, S. Takeda, E. Rotenberg, I. Matsuda, K. Horikoshi, J. Schaefer, C. M. Lee, S. D. Kevan, T. Ohta, T. Nagao, and S. Hasegawa, Instability and Charge Density Wave of Metallic Quantum Chains on a Silicon Surface, Phys. Rev. Lett. **82**, 4898 (1999).
[2] S. Chandola, K. Hinrichs, M. Gensch, N. Esser, S. Wippermann, W. G. Schmidt, F. Bechstedt, K. Fleischer, and J. F. McGilp, Structure of Si(111)-In Nanowires Determined from the Midinfrared Optical Response, Phys. Rev. Lett. **102**, 226805 (2009).
[3] A. A. Stekolnikov, K. Seino, F. Bechstedt, S. Wippermann, W. G. Schmidt, A. Calzolari, and M. Buongiorno Nardelli, Hexagon versus Trimer Formation in In Nanowires on Si (111): Energetics and Quantum Conductance, Phys. Rev. Lett. **98**, 026105 (2007).
[4] T. Tanikawa, I. Matsuda, T. Kanagawa, and S. Hasegawa, Surface-State Electrical Conductivity at a Metal-Insulator Transition On Silicon, Phys. Rev. Lett. **93**, 016801 (2004).
[5] S. J. Park, H. W. Yeom, S. H. Min, D. H. Park, and I. W. Lyo, Direct Evidence of the Charge Ordered Phase Transition of Indium Nanowires on Si(111), Phys. Rev. Lett. **93**, 106402 (2004).
[6] J. R. Ahn, J. H. Byun, H. Koh, E. Rotenberg, S. D. Kevan, and H. W. Yeom, Mechanism of Gap Opening in a Triple-Band Peierls System: In Atomic Wires on Si, Phys. Rev. Lett. **93**, 106401 (2004).
[7] Y. J. Sun, S. Agario, S. Souma, K. Sugawara, Y. Tago, T. Sato, and T. Takahashi, Cooperative structural and Peierls transition of indium chains on Si(111), Phys. Rev. B **77**, 125115 (2008).

[8] S. Riikonen, A. Ayuela, and D. Sánchez-Portal, Metal–insulator transition in the In/Si(111) surface, Surf. Sci. **600**, 3821 (2006).

[9] S. Wippermann and W. G. Schmidt, Entropy Explains Metal-Insulator Transition of the Si(111)-In Nanowire Array, Phys. Rev. Lett. **105**, 126102 (2010).

[10] W. G. Schmidt, S. Wippermann, S. Sanna, M. Babilon, N. J. Vollmers, and U. Gerstmann, In-Si(111)$(4 \times 1)/(8 \times 2)$ nanowires: Electron transport, entropy, and metal-insulator transition, Phys. Status Solidi B **249**, 343 (2012).

[11] E. Jeckelmann, S. Sanna, W. G. Schmidt, E. Speiser, and N. Esser, Grand canonical Peierls transition in In/Si(111), Phys. Rev. B **93**, 241407(R) (2016).

[12] E. Speiser, N. Esser, S. Wippermann, and W. G. Schmidt, Surface vibrational Raman modes of In/Si(111) (4×1) and (8×2) nanowires, Phys. Rev. B **94**, 075417 (2016).

[13] M. Chávez-Cervantes, R. Krause, S. Aeschlimann, and I. Gierz, Band structure dynamics in indium wires, Phys. Rev. B **97**, 201401(R) (2018).

[14] J. G. Horstmann *et al.*, Coherent control of a surface structural phase transition, Nature (London) **583**, 232 (2020).

[15] See Supplemental Material at http://link.aps.org/supplemental/10.1103/PhysRevLett.130.146901 for methods, supplemental results and movie, which include Refs. [9,14,16–26].

[16] Z. Wang, S. S. Li, and L. W. Wang, Efficient Real-Time Time-Dependent Density Functional Theory Method and Its Application to a Collision of an Ion with a 2d Material, Phys. Rev. Lett. **114**, 063004 (2015).

[17] W. H. Liu, Z. Wang, Z. H. Chen, J. W. Luo, S. S. Li, and L. W. Wang, Algorithm Advances and Applications of Time-Dependent First-Principles Simulations for Ultrafast Dynamics, Wires Comput. Mol. Sci. **12**, e1577 (2022).

[18] T. Frigge, B. Hafke, T. Witte, B. Krenzer, C. Streubuhr, and A. Samad Syed, V. Miksic Trontl, I. Avigo, P. Zhou, M. Ligges, D. von der Linde, U. Bovensiepen, M. Horn-von Hoegen, S. Wippermann, A. Lucke, S. Sanna, U. Gerstmann, and W. G. Schmidt, Optically excited structural transition in atomic wires on surfaces at the quantum limit, Nature (London) **544**, 207 (2017).

[19] W. H. Liu, J. W. Luo, S. S. Li, and L. W. Wang, Microscopic force driving the photoinduced ultrafast phase transition: Time-dependent density functional theory simulations of IrTe2, Phys. Rev. B **102**, 184308 (2020).

[20] W. H. Liu, J. W. Luo, S. S. Li, and L. W. Wang, The critical role of hot carrier cooling in optically excited structural transitions, npj Comput. Mater. **7**, 117 (2021).

[21] H. W. Liu, W. H. Liu, Z. J. Suo, Z. Wang, J. W. Luo, S. S. Li, and L. W. Wang, Unifying the order and disorder dynamics in photoexcited VO_2, Proc. Natl. Acad. Sci. U.S.A. **119**, e2122534119 (2022).

[22] S. Wall, S. Yang, L. Vidas, M. Chollet, J. M. Glownia, M. Kozina, T. Katayama, T. Henighan, M. Jiang, T. A. Miller, D. A. Reis, L. A. Boatner, O. Delaire, and M. Trigo, Ultrafast disordering of vanadium dimers in photoexcited VO_2, Science **362**, 6414 (2018).

[23] E. Matsubara, S. Okada, T. Ichitsubo, T. Kawaguchi, A. Hirata, P. F. Guan, K. Tokuda, K. Tanimura, T. Matsunaga, M. W. Chen, and N. Yamada, Initial Atomic Motion Immediately Following Femtosecond-Laser Excitation in Phase-Change Materials, Phys. Rev. Lett. **117**, 135501 (2016).

[24] N. K. Chen, X. B. Li, J. Bang, X. P. Wang, D. Han, D. West, S. B. Zhang, and H. B. Sun, Directional Forces by Momentumless Excitation and Order-to-Order Transition in Peierls-Distorted Solids: The Case of GeTe, Phys. Rev. Lett. **120**, 185701 (2018).

[25] C. Lian, S. J. Zhang, S. Q. Hu, M. X. Guan, and S. Meng, Ultrafast charge ordering by self-amplified exciton–phonon dynamics in $TiSe_2$, Nat. Commun. **11**, 43 (2020).

[26] C. Lian, Z. A. Ali, H. Kwon, and B. M. Wong, Indirect but efficient: Laser-excited electrons can drive ultrafast polarization switching in ferroelectric materials, J. Phys. Chem. Lett. **10**, 3402 (2019).

[27] A. Lucke, U. Gerstmann, T. D. Kuhne, and W. G. Schmidt, Efficient paw-based bond strength analysis for understanding the in/Si(111)$(8 \times 2) - (4 \times 1)$ phase transition, J. Comput. Chem. **38**, 2276 (2017).

[28] T. Frigge, B. Hafke, T. Witte, B. Krenzer, and M. Horn-von Hoegen, Non-equilibrium lattice dynamics of one-dimensional in chains on Si(111) upon ultrafast optical excitation, Struct. Dyn. **5**, 025101 (2018).

[29] C. W. Nicholson, A. Lucke, W. G. Schmidt, M. Puppin, L. Rettig, R. Ernstorfer, and M. Wolf, Beyond the molecular movie: Dynamics of bands and bonds during a photoinduced phase transition, Science **362**, 821 (2018).

[30] M. Chavez-Cervantes, G. E. Topp, S. Aeschlimann, R. Krause, S. A. Sato, M. A. Sentef, and I. Gierz, Charge Density Wave Melting in One-Dimensional Wires with Femtosecond Subgap Excitation, Phys. Rev. Lett. **123**, 036405 (2019).

[31] C. W. Nicholson, M. Puppin, A. Lücke, U. Gerstmann, M. Krenz, W. G. Schmidt, L. Rettig, R. Ernstorfer, and M. Wolf, Excited-state band mapping and momentum-resolved ultrafast population dynamics in In/Si(111) nanowires investigated with Xuv-based time- and angle-resolved photoemission spectroscopy, Phys. Rev. B **99**, 155107 (2019).

[32] S. Wall, B. Krenzer, S. Wippermann, S. Sanna, F. Klasing, A. Hanisch-Blicharski, M. Kammler, W. G. Schmidt, and M. Horn-von Hoegen, Atomistic Picture of Charge Density Wave Formation at Surfaces, Phys. Rev. Lett. **109**, 186101 (2012).

[33] L. Perfetti, P. A. Loukakos, M. Lisowski, U. Bovensiepen, H. Berger, S. Biermann, P. S. Cornaglia, A. Georges, and M. Wolf, Time Evolution of the Electronic Structure of 1T-TaS2 through the Insulator-Metal Transition, Phys. Rev. Lett. **97**, 067402 (2006).

[34] H. Schäfer, V. V. Kabanov, M. Beyer, K. Biljakovic, and J. Demsar, Disentanglement of the Electronic and Lattice Parts of the Order Parameter in a 1D Charge Density Wave System Probed by Femtosecond Spectroscopy, Phys. Rev. Lett. **105**, 066402 (2010).

[35] L. Rettig, R. Cortés, J. H. Chu, I. R. Fisher, F. Schmitt, R. G. Moore, Z. X. Shen, P. S. Kirchmann, M. Wolf, and U. Bovensiepen, Persistent order due to transiently enhanced nesting in an electronically excited charge density wave, Nat. Commun. **7**, 10459 (2016).

[36] S. Hellmann, T. Rohwer, M. Kalläne, K. Hanff, C. Sohrt, A. Stange, A. Carr, M. M. Murnane, H. C. Kapteyn, L. Kipp, M. Bauer, and K. Rossnagel, Time-domain classification of charge-density-wave insulators, Nat. Commun. **3**, 1069 (2012).

[37] B. Hafke, T. Witte, D. Janoschka, P. Dreher, F.-J. Meyer zu Heringdorf, and M. Horn-von Hoegen, Condensation of ground state from a supercooled phase in the Si(111)-$(4 \times 1) \rightarrow (8 \times 2)$-indium atomic wire system, Struct. Dyn. **6**, 045101 (2019).

[38] C. González, F. Flores, and J. Ortega, Soft Phonon, Dynamical Fluctuations, and a Reversible Phase Transition: Indium Chains on Silicon, Phys. Rev. Lett. **96**, 136101 (2006).

[39] T. Huber, S. O. Mariager, A. Ferrer, H. Schäfer, J. A. Johnson, S. Grübel, A. Lübcke, L. Huber, T. Kubacka, C. Dornes, C. Laulhe, S. Ravy, G. Ingold, P. Beaud, J. Demsar, and S. L. Johnson, Coherent Structural Dynamics of a Prototypical Charge-Density-Wave-to-Metal Transition, Phys. Rev. Lett. **113**, 026401 (2014).

[40] M. J. Neugebauer, T. Huber, M. Savoini, E. Abreu, V. Esposito, M. Kubli, L. Rettig, E. Bothschafter, S. Grübel, T. Kubacka, J. Rittmann, G. Ingold, P. Beaud, D. Dominko, J. Demsar, and S. L. Johnson, Optical control of vibrational coherence triggered by an ultrafast phase transition, Phys. Rev. B **99**, 220302(R) (2019).

[41] P. Beaud *et al.*, A time-dependent order parameter for ultrafast photoinduced phase transitions, Nat. Mater. **13**, 923 (2014).

[42] J. Zhang, C. Lian, M. Guan, W. Ma, H. Fu, H. Guo, and S. Meng, Photoexcitation induced quantum dynamics of charge density wave and emergence of a collective mode in 1T-TaS_2, Nano Lett. **19**, 6027 (2019).

[43] C. J. Sayers, H. Hedayat, A. Ceraso, F. Museur, M. Cattelan, L. S. Hart, L. S. Farrar, S. Dal Conte, G. Cerullo, C. Dallera, E. Da Como, and E. Carpene, Coherent phonons and the interplay between charge density wave and Mott phases in 1T-$TaSe_2$, Phys. Rev. B **102**, 161105 (2020).

[44] W. H. Liu, J. W. Luo, S. S. Li, and L. W. Wang, The seeds and homogeneous nucleation of photoinduced nonthermal melting in semiconductors due to self-amplified local dynamic instability, Sci. Adv. **8**, 27 (2022).

[45] C. González, J. Ortega, and F. Flores, Metal–insulator transition in one-dimensional In-chains on Si(111): Combination of a soft shear distortion and a double-band Peierls instability, New J. Phys. **7**, 100 (2005).